Pore-scale model for fluid injection and *in situ* gelation in porous media

Karsten E. Thompson
Department of Chemical Engineering, Louisiana State University, Baton Rouge, Louisiana 70803

H. Scott Fogler
Department of Chemical Engineering, The University of Michigan, Ann Arbor, Michigan 48109
(Received 1 October 1997)

We examine immiscible fluid displacement in a porous material for the case where a polymerization reaction occurs at the interface between two fluid phases. A three-dimensional sphere-based network model is used to study the process. An *in situ* reaction may affect the pore morphology, interfacial forces, or viscous forces, thereby altering the pressure distribution and displacement pattern. The amount and manner in which the displacement pattern is affected depends on competing rates of reaction versus convection. The model shows that at high-capillary-number displacements, a narrow range of reaction rates affects the displacement process, below which no effect is seen and above which the flow stops. As the capillary number decreases, this range widens but at the expense of the overall hydraulic conductivity. This phenomenon is explained using microscopic displacement patterns. An operating window can be drawn showing the flow and reaction domain in which one would expect an interfacial reaction of this type to affect fluid displacement. [S1063-651X(98)13805-9]

PACS number(s): 47.55.Mh, 47.70.−n

I. INTRODUCTION

This paper describes results from a network model study of the injection of a reactive fluid into a porous material to form an immobile polymer or gel phase. This phenomenon occurs, for example, during the injection of cross-linking polymers into an oil reservoir or the impregnation of fibers or powders by a polymer. In either of these applications, the final spatial distribution of the polymer affects the macroscopic properties of the material. Hence, it is important to understand the influence of various parameters on the reaction and injection process.

The experimental work leading to this investigation involved the injection and *in situ* reaction of a silica gel in consolidated porous media to study improved oil recovery. Experiments showed that gel does not coat or fill the void space uniformly. Rather, it deposits in specific sites within the medium, which are dictated primarily by the position of fluid interfaces during the delivery of reactants. The dynamics of immiscible displacement are normally governed by the balance between interfacial and viscous forces at the pore level. For this type of polymer injection, the displacement pattern is also affected by the *in situ* reaction, which continually changes the pore-space morphology. Because of the strong dependence on pore-scale events, the displacement was modeled using a sphere-based network model that accounts for pore-scale disorder and interconnectivity.

A. Previous experimental results

The goal of previous experimental work was to develop techniques to alter multiphase permeability in porous media using polymers or gels. One proposed mechanism for polymer delivery in oil-field operations is the injection of a reactive organic phase that will polymerize upon contact with an aqueous phase. This technique provides a natural selectivity so that the cross-linked polymer forms only where water is present. A model experimental system was used to study this process; the reactive organic-phase fluid was a solution of tetramethyl orthosilicate (TMOS) in an inert hydrocarbon, which undergoes an interfacial reaction upon contact with water to form silicic acid and finally silica gel (in the aqueous phase) [1].

The reaction rate for most TMOS reactions can be controlled by a combination of solution *p*H and a choice of alcohol catalyst [2]. Unfortunately, within the constraints of the experimental system the reaction rate cannot be varied gradually. A fast reaction rate can be obtained using ammonium hydroxide and octanol, in which case silica gel forms on the order of seconds so that the time scales for reaction and injection are similar. At a neutral *p*H a cross-linked silica gel forms on the order of hours, so experiments were performed by injecting the reactant and allowing it to react for 24 hours. As one might expect, the more rapid formation of silica gel during injection causes significant losses in permeability (two to three orders of magnitude in consolidated media). When the reaction rate is slow, the final permeabilities are usually two to ten times lower than before treatment. For either reaction rate, the final distribution of silica gel is nonuniform, causing disproportionate changes in the aqueous versus organic-phase permeabilities [1,3]. These observations, along with the inability to effectively control the reaction rate, prompted a pore-scale investigation of the dynamic process to better understand the mechanism of injection and gelation and the subsequent effect on the hydraulic conductivity of the porous material.

B. Requirements of the model

The complexity of the experimental process dictates that numerous simplifications be made for the modeling. The approach used in this work is to include a rigorous model of the

fluid displacement while simplifying the reaction chemistry considerably. Hence, the basic mechanism to be modeled is as follows. A nonwetting fluid with a time-dependent interfacial reaction is injected into the medium; the extent of reaction dictates the local wetting-phase viscosity, and pore throats ultimately lose all conductivity as a result of gelation.

Because pore-scale events are crucial to understanding the process, a number of characteristics were required of the model. These characteristics included the ability to reproduce fundamental displacement phenomena and predict macroscopic parameters after the injection process. A network model was chosen as a means to effectively incorporate pore-scale disorder, heterogeneity, and interconnectivity, which are important to displacement processes [4,5]. Recent advances have demonstrated the ability to effectively predict macroscopic parameters using network models of realistic geometries [6,7].

Bench-scale rate studies were performed using a TMOS solution reacting at an aqueous interface. These studies showed that the interfacial reaction rate to form silicic acid from TMOS depends on interface area, *p*H, salinity, TMOS concentration, and temperature. The overall reaction to form silica gel depends on the interfacial reaction rate to silicic acid, as well as the ratio of phase volumes, and presumably the rates of diffusion of TMOS to the interface and diffusion of the reactants away. Many of these parameters could not be evaluated effectively in the complex pore structure. Hence, the chemistry of gelation is modeled as a simple function of the time that an interface remains in a pore throat. The role of the network model is to determine the location of all the fluid interfaces during the displacement process.

C. Network models

Network models are usually comprised of two-dimensional (2D) or 3D networks of cylindrical bonds. Regular lattice arrangements are most prevalent, although methods have been proposed to vary the coordination number and bond lengths [4,5,8]. The modeling described here uses a three-dimensional packing of spheres as the foundation for the physical network [6,7]. This technique is well suited for granular porous media because the spatial correlation of pore sizes is included naturally, the distribution of pore sizes comes from specifying a grain-size distribution rather than inference from porosimetry, the pore-scale morphology for granular media is not compromised, and no scaling parameters are needed. This technique is a promising method by which macroscopic parameters can be evaluated from a description of pore-scale phenomena.

Solving for flow in a network structure requires that one have a mathematical expression for flow rate versus pressure drop in the network bonds. (For instance, in networks with cylindrical bonds, the Hagen-Poiseuille equation [9] for laminar flow in a tube is usually used.) For sphere-based networks, which are used here, the procedure is somewhat involved. First, a Delaunay tessellation is employed in order to discretize the sphere pack into a series of pores and pore throats. The throats have irregular cross sections and a converging diverging geometry. Hence, the assignment of pore-throat conductivities must include either a complex numerical solution, or some manner of approximation. In the model used for this work, a flow rate versus pressure-drop relationship for flow through each irregular cross section is calculated numerically. These results are superimposed on equations for creeping flow through hyperboloids of revolution in order to account for the converging-diverging shape (details of this process are given in Ref. [7]). Once throat conductivities have been assigned, they are used with the nodal pressures to write equations for flow through each pore. The net flow is zero for interior pores and is either unknown or part of a boundary condition for inlet or outlet pores. The result is a system of linear algebraic equations for which the pressure is unknown in all interior pores.

The literature contains numerous models for multiphase flow in networks. Nonwetting phase injection (or drainage) is one of the easiest multiphase phenomena to model and, hence, has been widely studied (other published articles contain comprehensive references to past work [10,11]). The most common algorithms are pseudostatic displacements, which are the same as invasion percolation. They are valid only for conditions where viscous forces are not important. Models for viscous displacements are more complex because the governing equations are nonlinear. The algorithm developed for this work is valid for both capillary- and viscous-dominated conditions and the range in between, which allows investigation of how the capillary and viscous forces interact with the gelation reaction. The algorithm is described only briefly below, but a more extensive discussion on pore-scale modeling of displacement phenomena can be found in Lenormand *et al.* [12].

II. IMMISCIBLE DISPLACEMENT

Because the injection-reaction process depends so strongly on pore-scale events, we begin with a brief discussion of the governing phenomena for immiscible displacements, followed by some of the challenges for modeling this process.

A. Displacement mechanisms

The displacement pattern during injection of a nonwetting fluid into a porous medium is a strong function of pore-size distribution, pore shapes, fluid viscosities, injection rate, and the interfacial tension. For a fixed porous medium and fluid pair, the displacement pattern can be correlated with the dimensionless capillary number [5,12,13]

$$N_{\mathrm{Ca}}=\frac{\mu v}{\sigma}. \tag{1}$$

Here the capillary number is defined with respect to spatially averaged parameters: μ is the injected phase viscosity, v is the superficial velocity, and σ is the interfacial tension. The capillary number indicates the relative importance of viscous to interfacial forces.

At the pore scale, a drainage front advances by a series of discrete invasions. Each one occurs when the local capillary pressure is sufficient so that the interface can curve to conform to the smallest constriction imposed by the bounding solid. In a network model, the invasion steps are also discrete. In order to decide when an invasion occurs, one must assign a capillary entry pressure to each pore throat based on

its geometry. This parameter is usually calculated using the equilibrium Young-Laplace equation, which requires knowledge of the interface's radii of curvature in a pore throat. In a granular medium or in the model sphere pack used here, local interfaces take on a saddle shape so that the radii of curvature are different in magnitude and sign. In a pack of spheres, the pore throats are the spaces between three neighboring spheres whose centers make a triangle. One radius of curvature is estimated by the inscribed circle that fits into this void. The other is estimated as a function of the average diameter of the bounding spheres (which dictates the opposing radius of curvature on the saddle as the interface is squeezed into the throat).

Once capillary entry pressures are assigned, the nonwetting phase can be advanced into the network by a number of techniques. For pseudostatic displacements, the interface always advances where the capillary entry pressure is smallest, and the inlet capillary pressure rises or falls accordingly since there is no pressure drop in the injected phase. When viscous forces are important, the displacement algorithm becomes more complicated because choosing the sites to advance the interface requires a knowledge of the contributions to capillary pressure from internal viscous forces, as well as the injection pressure. Predicting the viscous pressure drops requires a solution of the flow pattern, which in turn requires a knowledge of the invaded pores. Consequently, the algorithm must be solved iteratively or by nonlinear techniques [12–14]. In some cases, this complication is ignored, and the pores to be invaded are chosen from the capillary pressures during the previous step [15], which provides for a faster and more stable solution, but the invasion pattern is approximate. In the model described here, an iterative technique is used to overcome this approximation.

Numerous other issues are important to moving-interface problems, such as snap-off or the validity of using constant radii of curvature. Snap-off depends on the local aspect ratio, pore shape, wetting-phase conductivity, and local viscous forces; while it can occur during nonwetting-phase invasion, it is infrequent when the nonwetting-phase saturation increases monotonically. For this reason, snap-off is neglected. The other approximations made here are quite standard in network modeling, and are required so that the solution of the model remains tractable.

From the above pore-scale arguments it becomes evident how the macroscopic capillary number contributes to the displacement pattern. When viscous forces are very small, the displacement pattern is tortuous with many dead-end pathways because fingers advance only until a small pore is encountered, causing flow to branch out elsewhere. When viscous forces are high, capillary pressures rise behind the displacing front so that small pores may be invaded after the front has passed. Plug-flow displacements occur at high capillary numbers.

The final issue discussed in this section is the wetting-phase conductivity and saturation. In complex media (e.g., consolidated sands) the wetting phase never becomes isolated. In sphere packs it can become essentially isolated in the form of pendular rings. In a network model, the decision whether to maintain wetting-phase conductivity in invaded pores dictates whether wetting-phase ganglia can become trapped or whether they continue to drain after a displacing front has passed. In this model, pores always contain wetting fluid; the local saturation is related to the local capillary pressure using simple formulas for the volume of pendular rings as a function of interface curvature [16]. The local throat conductivity to the nonwetting phase immediately after displacement is taken to be 95% of the total conductivity. It then increases to 100% in proportion to the nonwetting-phase saturation. The wetting-phase conductivity is calculated simply as the difference between the nonwetting phase and absolute conductivity. This mathematical relation is arbitrary and not intended to be quantitatively correct. It is instead designed to allow the existence of a small wetting-phase conductivity. The high nonwetting-phase conductivity after displacement is consistent with relative permeability studies.

B. Quasi-steady-state modeling

The displacement algorithm uses a quasi-steady-state assumption (QSSA) to model the displacement patterns over a broad range of capillary numbers, which is effective for predicting unsteady behavior such as changes in injection pressure or the slow drainage of wetting films. It is described briefly here and shown in detail in Thompson [14].

The inlet boundary conditions are found by specifying the total flow rate of injected fluid (meaning the injection pressure will vary with time). Displacement occurs by modeling a number of discrete time increments during each of which a QSSA solution for flow of the injected and displaced fluids is found. Each QSSA solution may include the invasion of any number of pores at the fluid interface. The decision to invade depends on the local capillary pressure, while the invasion rate into each pore depends on local pressures and throat conductivities. The time step during which each QSSA solution is valid continues until most of the newly invaded pores attain their minimum capillary saturation. Because each pore is invaded at a different rate, some will fill before the time step is finished. Once a pore is filled during the current time step, advance of that interface is halted until the others fill. This procedure mimics the known invasion phenomenon where pores are filled in discrete steps called Haines jumps. The mathematics of the algorithm simply allows a group of pores to jump together. A time step ends when newly invaded pores are filled, unless, one or more pores are filling slowly (when downstream conditions do not allow the wetting phase to drain quickly). In this case a new time step is begun while the slow pores are still being invaded so that some pores become filled with displacing fluid over the course of many time steps.

A significant difference between this and many other algorithms is that the capillary pressure in a pore must always correspond to the saturation in that pore. This requirement causes some numerical difficulty because the pressures in each phase are determined independently, yet they dictate the local flow rates. These local flow rates in turn affect the saturation at the end of a time step, which must agree with the pressures that were determined. Convergence of this system of constraints is sometimes slow or unstable, and additional research must be performed to facilitate rapid convergence. However, the algorithm is consistent with the real phenomenon, in which the wetting phase continues to drain slowly as the inlet capillary pressure increases and the sys-

tem approaches steady state. At a true steady state, a capillary pressure gradient will exist through the network and the pressure gradient in the hydraulically connected displaced phase will be zero.

To implement the displacement mechanism described above, the algorithm is divided into two components. The first is the invasion sequence algorithm, which determines what pores are to be invaded during the current time step. An estimate of the pressures is made using information from the previous time step along with expected changes. The estimate is compared with the updated solution for pressure, which requires the second component of the algorithm: the quasi-steady-state solution for the pressures and flow rates. Once a correct QSSA pressure distribution is obtained, the values are used to advance the fluid by a time step. Most of the details of the numerical process will not be described here. However, we describe the bookkeeping that is used to keep track of the evolving saturation pattern. Pores along the advancing front are divided into three categories.

(i) Uninvaded pores: These pores are still filled with water, and if they are the next ones invaded, then the oil-phase conductivity of at least one throat must be set to a nonzero value.

(ii) Partially invaded pores: These pores are relatively rare because invasion on the pore scale usually occurs in a discrete jump to the minimum capillary saturation. However, in cases where the evacuation of displaced fluid from that pore is slow, but the capillary pressure has been overcome, the invasion occurs at a leisurely pace dictated by the flow out of the pore.

(iii) Completely invaded pores: These pores have been invaded and have a local capillary pressure that is equal to or above the minimum value. However, the net flow of the displacing phase in these pores may still be nonzero during a time step in order to maintain consistency between the capillary pressure and saturation within a pore. The flow rates of injected and displaced fluids must, of course, balance one another.

The pressure distribution in each phase is solved by the Gauss-Seidel method with relaxation; over- and under-relaxation are used depending on stability during the current time step. For single-phase flow the equations are forced to converge on zero net flow in each pore (mass conservation). For two-phase flow the equations are forced to converge on an equal and opposite net flow of each phase. The capillary pressure in each pore (i.e., the calculated pressure difference between the two phases) must agree with the current saturation for that pore.

C. Model results for fluid injection

The network model used for this work is a sphere-based model. Small sphere packings were used for the multiphase studies because the algorithm is computationally intensive; for the results shown here about 1500 spheres were used to create the bed, and an interior section containing 903 Delaunay cells (pores) formed the network. The mean-sphere diameter was 100 μm with a standard deviation of 25 μm. The displaced and injected fluid viscosities were 1.0 and 2.0 cP, respectively. The interfacial tension was 50 dyn/cm. Injection rates were varied over four orders of magnitude between 0.2 and 0.0002 cm^3/s. All of the above parameters were chosen to represent the experimental studies mentioned previously except for the standard deviation in sphere size, which was chosen arbitrarily (the experimental studies were performed in artificial consolidated ceramic media, while the model is for unconsolidated spherical packings).

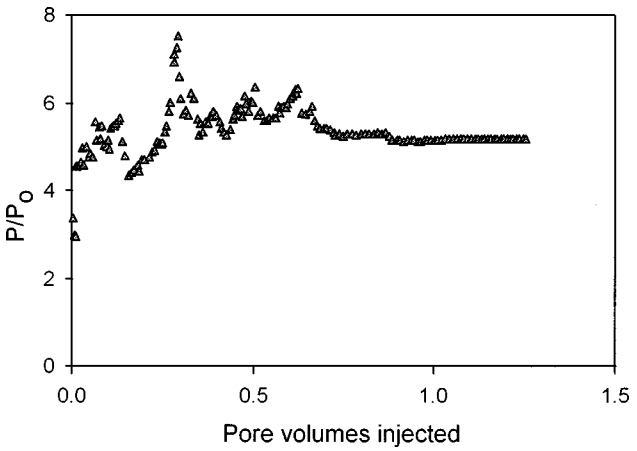

FIG. 1. Displacement at a low flow rate.

The transient pressure response is an important parameter for most processes and is vastly different at the two extremes represented by the capillary number. The pressure is shown as P/P_0, a dimensionless ratio of current inlet pressure over inlet pressure for single-phase flow of the displaced fluid at the same rate (note that because the magnitude of the reference pressure is proportional to the injection rate, a high dimensionless pressure does not necessarily correspond to a high absolute injection pressure). At very low injection rates the interfacial forces dominate and the inlet pressure is nearly equal to the capillary pressure required to invade the largest currently available pore. Because the invasion front may break through a small pore into regions where the capillary entry pressures are lower, the inlet pressure oscillates during injection as shown in Fig. 1. These oscillations are more pronounced for a small medium because of the limited number of choices for invasion during any given time step. Typically they would not be seen in a large medium such as one used for experimental displacements. Alternatively, when viscous forces dominate, the inlet pressure is not affected by interfacial forces, but rather, it represents the sum of the viscous pressure drops within each phase. For a high injection rate, the displacement is nearly plug flow. Hence, the inlet pressure is the series contribution from the two viscous pressure drops. This behavior is seen in Fig. 2, which shows a nearly linear increase in pressure until breakthrough. The pressure drop increases in proportion to the viscosity ratio of the injected versus displaced fluid.

The displacement efficiency is higher for injections at high capillary numbers. This behavior can be quantified by examining the displaced fluid saturation at breakthrough and steady state for the four flow rates shown in Table I. This trend is also seen by simulating external residence time distributions (RTDs) in the injected phase once steady state has been reached. The RTD is important because the average residence time provides an indication of the injected-phase

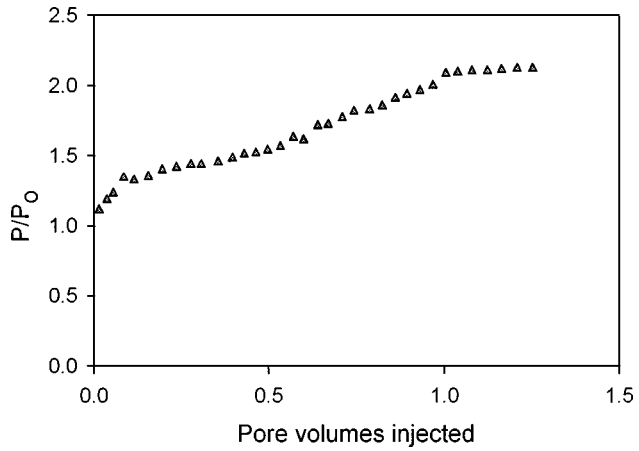

FIG. 2. Displacement at a high flow rate.

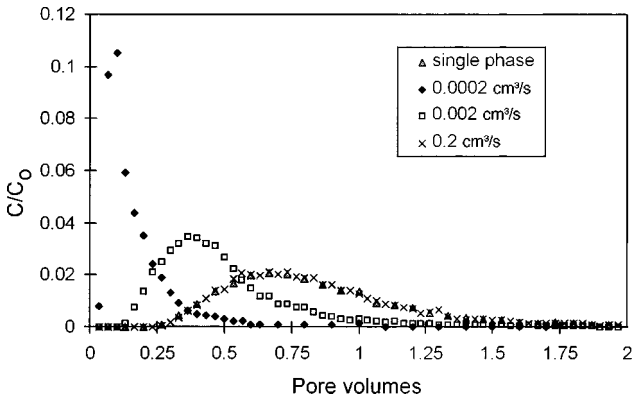

FIG. 3. Injected-phase RTDs after breakthrough. C/C_0 is the outlet tracer concentration over the injected concentration.

saturation (or more specifically, the saturation of the conducting backbone), and the shape of the distribution is a qualitative indicator of the range of pore sizes used to transport the injected phase. Figure 3 shows RTDs for steady flow of the injected fluid after displacement at three different rates as compared to the RTD for single-phase flow (saturation $=1$). After the high capillary number displacement, the injected fluid occupies essentially the entire bed. For lower injection rates, the final saturation of the displacing fluid decreases and the tracer peaks become narrower. The latter trend indicates that a smaller size distribution of pores is sampled and that fewer flow pathways are available.

During experiments, steady-state flow is not achieved until well after the initial breakthrough of the displacing fluid from a core plug or packed bed. During the time between breakthrough and steady state there is a slow drainage of the wetting films. The algorithm used here maintains the continuity of the wetting phase and allows for drainage in response to increasing capillary pressures throughout the network. Macroscopically, the model predicts a fraction of displaced phase in the effluent for some time after breakthrough, as well as a slight decrease in the injection pressure while this occurs. These phenomena are consistent with what is observed in real situations.

Previous studies show the effect of the capillary number during drainage displacements graphically [12,15]. Similar images are shown here to better illustrate the phenomenon described below, for the reactive system. Because there is not an effective way to graphically represent fluid displacement in 3D sphere packs, bonds are drawn between pores and the network is projected onto a 2D plane. Figure 4 shows 2D projections of the network for displacements of 0.4 PV (pore volumes) injected fluid. The three images are for capillary numbers of 0.3, 0.003, and 0.0003. The darker lines represent bonds that have been invaded by displacing fluid. The nearly plug-flow behavior at high injection rates is evident, while the low injection flow rates create tortuous paths with many dead ends.

TABLE I. Injected-phase saturation for decreasing injection rates.

Flow rate (cm^3/s)	N_{Ca} (dimensionless)	Displacing-phase saturation	
		Breakthrough	Steady state
0.2	0.3	0.906	0.993
0.02	0.03	0.811	0.954
0.002	0.003	0.582	0.728
0.0002	0.0003	0.401	0.401

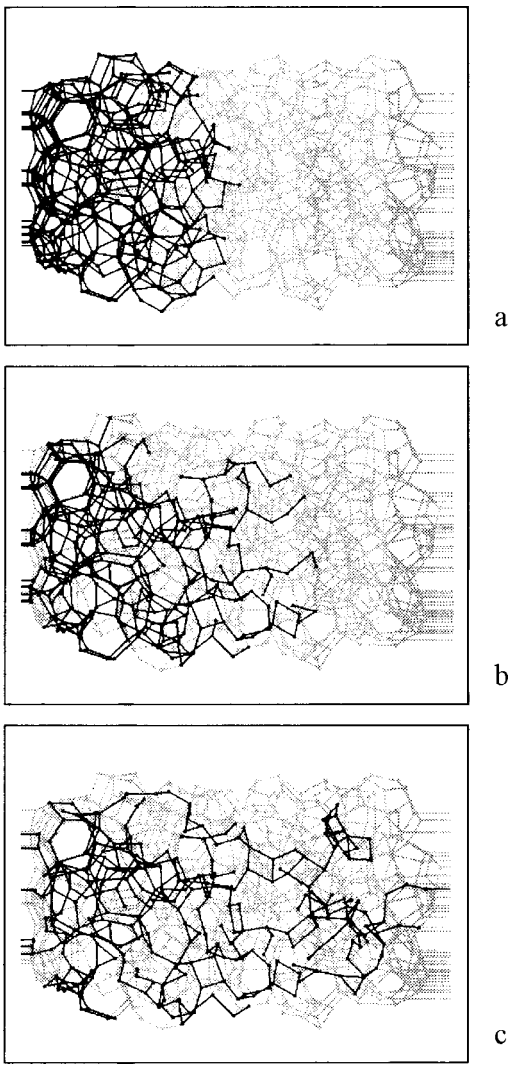

FIG. 4. Graphical depiction of immiscible displacement after 0.4 PV injected at (a) $N_{Ca}=0.3$, (b) 0.003, (c) 0.0003.

III. MODELING FLOW WITH REACTION

Clearly the injection of a polymerizing fluid into a porous medium will change the fundamental displacement mechanism that was described above. Changes in viscosity affect the capillary pressure distribution, while the formation of polymer or gel in pore throats changes the basic pore topology. Because the process modeled here involves an interfacial reaction, the time that an interface spends in any given throat affects whether it is able to move at a later time, which is indeed the phenomenon that has been observed experimentally. The combined effects of the reaction, viscous forces, and interfacial forces lead to different displacement mechanisms than are observed in cases having no reaction.

A. Including reactive flow in the network model

Although some of the rate parameters for the TMOS reaction have been quantified, the complexity of the whole reaction sequence precludes incorporating a rigorous description into the network model. Instead, the model allows the viscosity of the wetting phase to increase with time in the neighborhood of an interface. (This mechanism approximates the formation of silica gel in the aqueous phase.) A general exponential expression was used to describe the change in viscosity:

$$\mu = \mu_0 + \alpha\left(1 - \frac{1}{e^{k(t-t_{\text{inv}})}}\right). \tag{2}$$

The parameter k is used to vary the reaction rate in the model studies. The parameter α was chosen as 10^4 (meaning the gel attains a viscosity of approximately 10 000 times the original displaced-phase viscosity). In the numerical scheme, pore throats are closed after the viscosity of adjoining pores reaches some limiting value. While this analysis is somewhat simplistic, it provides for a mechanism that resembles what was observed experimentally for the rapidly reacting silica gel in visual micromodel studies (see Thompson and Fogler [1]).

As in the previous section, the transient displacements are plotted using the dimensionless injection pressure versus time or injected pore volumes. However, changes in injection pressure reflect polymerization of the injected phase (which blocks fluid flow) as well as changes in viscosity and relative permeability. As one would anticipate, the slow injection of a reactive fluid causes a larger increase in the dimensionless pressure because the fluid is given a longer time to react as it flows into the porous material. It is desirable to remove this effect from the analysis so that the injection rate can be used to control the macroscopic capillary number. Accordingly, the reaction rate is shown below as the product of k [from Eq. (2)] and the space-time (or average residence time)

$$\text{Da} = k\tau. \tag{3}$$

This parameter is the Damkohler number for a first-order reaction. Its physical meaning for this application is simply the extent of reaction on a pore-volumes-injected basis. Subsequent data are shown using the scaled reaction parameter Da.

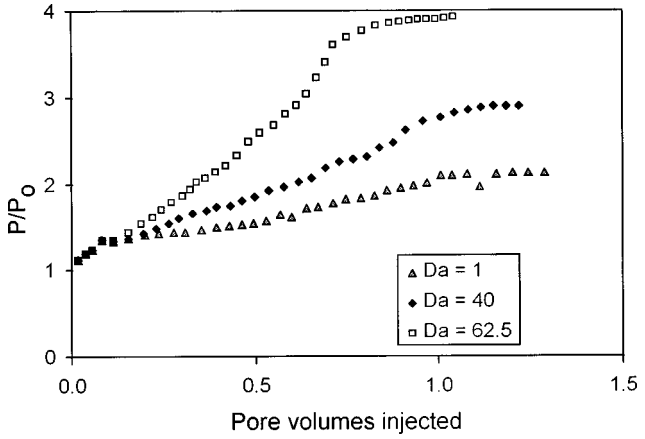

FIG. 5. Pressure response versus injected volume at various values of Da for high flow rates.

B. Effect of reaction rate

The reaction rate for gelation was varied in order to understand its effect on injection and placement of the gel. Note that for an efficient displacement without reaction the dimensionless pressure will rise to a value of just over 2.0, reflecting the change in viscosity from 1 to 2 cP. For a less efficient displacement (slow injection rate), the dimensionless pressure rises to a larger value reflecting changes in both viscosity and relative permeability. Bearing this in mind, the injection pressure without reaction will be used as the baseline to compare with other reacting displacements at that injection rate.

Figure 5 shows the transient injection pressure for a flow rate of 0.2 cm^3/s at three different reaction rates. The reaction rate of Da = 1.0 is nearly identical to the baseline with no reaction. As the reaction rate increases, the rate of pressure increase and the final pressure are both higher. The reaction rate Da = 62.5 is the maximum rate that could be accommodated without completely losing conductivity (injection pressure goes to infinity).

Figures 6 and 7 show equivalent plots for flow rates of 0.02 and 0.002 cm^3/s, respectively. In these runs, the highest reaction rates shown are also the maximum rates that still allow for fluid injection. They also show larger pressure increases as the polymerization rate is increased, which is not

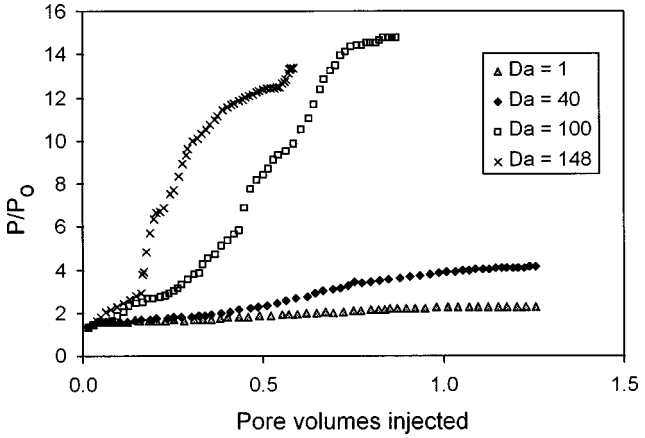

FIG. 6. Pressure response versus injected volume at various values of Da for moderate flow rates.

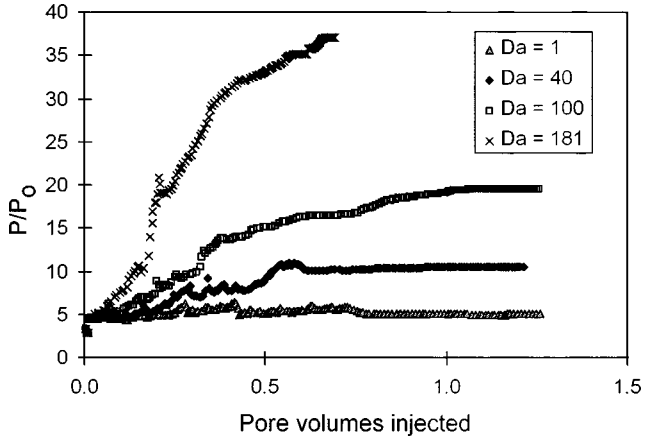

FIG. 7. Pressure response versus injected volume at various values of Da for low flow rates.

surprising. However, two other effects are worth noting. First, as the capillary number decreases (injection rate decreases), the maximum Damkohler number at which fluid can be injected increases. Second, the dimensionless injection pressure *at this maximum reaction rate* is higher for these slow injection rates.

The trends described above were analyzed at five injection rates between 0.002 and 0.2 cm^3/s. The results are combined in Fig. 8 to show the breakthrough pressures versus the polymerization rate for each different injection rate. The breakthrough pressure is the recorded injection pressure (dimensionless) at the time that the injected fluid reaches the outlet. This pressure does not necessarily correspond to steady state, but it is a good basis for comparison. The combination of runs shows the overall trend described above: slower injection rates accommodate higher Damkohler numbers before flow is stopped, but at the expense of hydraulic conductivity.

C. Mechanistic arguments

The mechanism for the phenomena described above is explained by pore-level arguments. First, recall how a displacement pattern varies with injection rate (or equivalently, the capillary number): high injection rates cause a plug displacement where the front advances in a steady, methodical manner into all the pore space. At low injection rates, the displacement pattern is tortuous with many dead ends. The latter pattern evolves because the displacement front explores various pathways in search of the lowest resistance; when a small pore throat is encountered, a branch somewhere else in the displaced network advances.

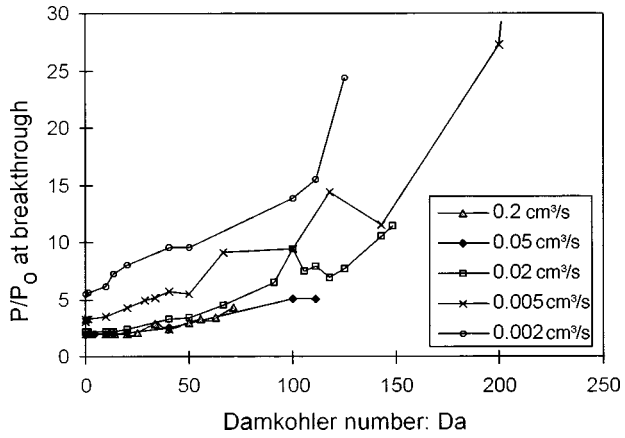

FIG. 8. Increasing flow resistance as injection rate decreases and Da increases.

Now consider a high injection rate with polymerization occurring at the advancing front. The displacement pattern is nearly plug flow so all interfaces advance at nearly the same rate. There is a reaction rate below which no interfaces remain stationary long enough for the reaction to have an effect on displacement. There is also a rate above which no interface advances quickly enough to ''outrun'' the reaction. There is a range between these maximum and minimum rates that is affected by the reaction. However, because all interfaces advance at nearly equal rates for high capillary numbers, this range is small.

Consider the opposite extreme: a capillary-dominated displacement at a very low injection rate. Because of the branchlike displacement pattern, where fingers of fluid are pushed into a region and then pause while other lower-resistance routes are explored, interfaces can remain stationary for a long time. Hence, even a slow gelation reaction can prevent the later advance of an interface that paused and then became frozen in place by the reaction. By a similar argument, a single advancing finger moves much more rapidly than the high-capillary-number front *with respect to the volume of fluid injected*. Because the reaction rate is scaled with pore volumes injected, a very high value of Da is required to shut off flow.

We now make a couple of notes in regard to these last arguments. For a low-capillary-number displacement with a reaction rate near or equal to the maximum (i.e., $Q=0.002$ and $Da=181$ in Fig. 7), side branches are quickly blocked by gel. Hence, there can be no backtracking to find a path of lower resistance once the tip of the finger encounters a high-capillary resistance. This effect is twofold. First, the displacing finger is highly tortuous but with few branches (confirmed by pictorial output from these runs). Second, because the displacing finger cannot backtrack, the final conductive channel most likely has a high resistance to flow. This conclusion explains the high dimensionless pressure drops that are seen for low-flow-rate displacements with moderate to high gelation rates.

IV. DISCUSSION

It is clear that a competition exists between the viscous forces (which cause pore throats to be invaded after a front passes) and the reaction rate (which causes pore throats to close if an interface remains static for an extended period of time). This effect causes the Damkohler number dependence shown in Figs. 5–7. In this paper, this phenomenon was shown for a unique placement mechanism where the gel or polymer forms via an interfacial reaction. However, the Damkohler number is known to govern other flow and reaction processes [17], and we would expect that it would be useful in characterizing other processes involving reactive polymer flows in porous media (e.g., material impregnation).

From the results shown in Sec. III we note that for all injection rates there exist both a lower reaction rate where

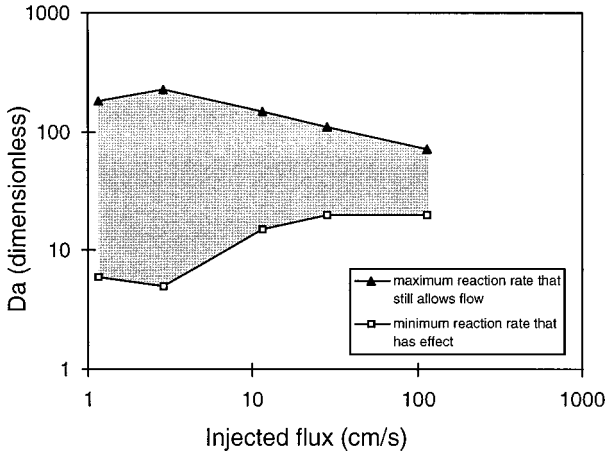

FIG. 9. Operating window where gelation reaction affects injection: Da versus superficial velocity.

fluid injection is not affected by the reaction and a high reaction rate where flow is stopped because the porous medium's conductivity is lost. Furthermore, the mechanistic arguments given in Sec. III C explain that this range between the lower and upper limits becomes larger as the rate of fluid injection decreases. This information is consolidated on a single plot in Fig. 9, which shows an operating window for this process. The scaled reaction rates Da at which these limits occur is shown as a function of the volume flux (or superficial velocity) of the injected fluid. The operating window between these lines is the region in which the placement of polymer is affected by the reaction rate.

One should note that the simulations shown here were performed all on the same network. (Other networks were used in order to check that the general trends were consistent.) This choice was made in order to isolate the effects of reaction and displacement rather than the morphology and heterogeneity of the porous media. However, it is expected that both small- and large-scale heterogeneity would strongly affect the injection-reaction process, especially for multiphase systems as described here.

Finally, it is noted that the most useful way of evaluating the effects of a gel treatment is usually by some macroscopic parameter, the choice of which depends on the process of interest. For applications in oil production this parameter would be the multiphase permeability. The network model has been used effectively for the prediction of averaged macroscopic behavior. Examples can be found in Thompson [14].

[1] K. E. Thompson and H. S. Fogler, SPE Production and Facilities **10**, 130 (1995).
[2] C. J. Brinker and G. W. Scherer, J. Non-Cryst. Solids **70**, 301 (1985).
[3] K. E. Thompson and H. S. Fogler, SPE J. **2**, 350 (1997).
[4] G. R. Jerauld, J. C. Hatfield, L. E. Scriven, and H. T. Davis, J. Phys. C **17**, 1519 (1984).
[5] M. Blunt and P. King, Phys. Rev. A **42**, 4780 (1990).
[6] S. Bryant and M. Blunt, Phys. Rev. A **46**, 2004 (1992).
[7] K. E. Thompson and H. S. Fogler, AIChE. J. **43**, 1377 (1997).
[8] G. N. Constantinides and A. C. Payatakes, Chem. Eng. Commun. **81**, 55 (1989).
[9] R. B. Bird, W. E. Stewart, and E. N. Lightfoot, *Transport Phenomena* (Wiley, New York, 1960).
[10] G. R. Jerauld and S. J. Salter, Transp. Porous Media **5**, 103 (1990).
[11] M. J. Blunt, SPE J. **2**, 70 (1997).
[12] R. Lenormand, E. Touboul, and C. Zarcone, J. Fluid Mech. **189**, 165 (1988).
[13] J. Koplik and T. J. Lasseter, Soc. Pet. Eng. J. **22**, 89 (1985).
[14] K. E. Thompson, Ph.D. thesis, University of Michigan, Ann Arbor, 1996.
[15] M. Blunt and P. King, Transp. Porous Media **6**, 407 (1991).
[16] W. Rose, J. Appl. Phys. **29**, 687 (1958).
[17] M. L. Hoefner and H. S. Fogler, AIChE. J. **34**, 45 (1988).